buildings

MDPI

Article

Design Methods of Aluminium Pin-Ended Columns with Topology-Optimised Cross-Sections

Mehmet Ali Güler [1], Aykut Artac [2], Bora Yildirim [2] and Konstantinos Daniel Tsavdaridis [3,4,*]

[1] College of Engineering and Technology, American University of the Middle East, Egaila 54200, Kuwait; mehmet.guler@aum.edu.kw
[2] Department of Mechanical Engineering, Hacettepe University, Ankara 06800, Türkiye; boray@hacettepe.edu.tr (B.Y.)
[3] Department of Engineering, School of Science & Technology, City, University of London, Northampton Square, London EC1V 0HB, UK
[4] International Advanced Science and Technology Research Organization (IROAST), Kumamoto University, Kurokami, Kumamoto 8608555, Japan
* Correspondence: konstantinos.tsavdaridis@city.ac.uk

Abstract: This paper presents a numerical study of topology-optimised pin-end aluminium alloy columns using finite element analysis (FEA). The FEA models integrate geometric imperfections and material nonlinearity, and are validated against experimental findings from the existing literature. ABAQUS v.6.15 (release 2020) is used in preparing the FEA models and obtaining the analysis results. Furthermore, modern design methodologies including Eurocode 9, the direct strength method (DSM), and the continuous strength method (CSM) are employed to assess the maximum load capacity of such columns. Parametric investigations encompass diverse parameters such as varied cross-sections, column lengths, and global and local imperfections. By analysing a total of 288 FE models, incorporating 16 column cross-sections across two lengths with nine distinct imperfections, this study compares results with those derived from modern design methodologies. Thus, this research elucidates the behaviour of novel cross-sections and the application of contemporary design techniques in their analysis.

Keywords: aluminium; columns; FE analysis; topology optimisation; DSM; CSM

Citation: Güler, M.A.; Artac, A.; Yildirim, B.; Tsavdaridis, K.D. Design Methods of Aluminium Pin-Ended Columns with Topology-Optimised Cross-Sections. *Buildings* **2024**, *14*, 3588. https://doi.org/10.3390/buildings14113588

Academic Editors: Francisco López-Almansa and Eric M. Lui

Received: 17 September 2024
Revised: 29 October 2024
Accepted: 11 November 2024
Published: 12 November 2024

1. Introduction

In recent years, the utilisation of aluminium columns in both civil and aerospace engineering has experienced significant growth, propelled by technological innovations and a steadfast commitment to sustainability, efficiency, and performance. This surge in usage underscores the inherent versatility and advantages offered by aluminium alloys, which have become indispensable in a wide array of structural applications. Aluminium, one of the most abundant elements on Earth, and renowned for its corrosion resistance, favourable strength-to-weight ratio, and similarities in design with stainless steel, has emerged as a preferred material choice in various industries (Georgantzia et al. 2021) [1]. Builders and developers are incorporating aluminium columns into green building projects to meet sustainability goals and reduce carbon footprints due to their light weight compared to steel (almost 2.5 times less). Moreover, innovations in fabrication technologies, such as extrusion and 3D printing, have expanded the design possibilities for aluminium members in civil engineering applications compared to their steel counterparts due to the lower energy requirement for manufacturing. Complex geometries and custom profiles can be produced, allowing for more efficient structural designs and optimised material usage. Furthermore, in regions prone to seismic activity, aluminium columns are preferred for their ductility and ability to withstand dynamic loads. However, despite their numerous benefits, the inherent characteristics of aluminium alloys, such as lower stiffness compared

to steel alloys, greater susceptibility to buckling compared to steel, and having fatigue characteristics that differ from those of steel, necessitate careful consideration in design. The current lack of comprehensive design codes and standards for aluminium structures can lead to uncertainties in design methodology and safety factors. This necessitates meticulous analysis and design considerations, particularly in structural applications where load-bearing capacity is paramount. One example would be the instability causing the reduction in the load-bearing capacity of aluminium columns under axial compressive loading.

Recently, numerous studies have explored compression members constructed from cold-formed steel (CFS), particularly those with perforations, generating a substantial amount of data to guide standards in the design of steel columns. Therefore, before delving into the available literature on aluminium columns, we present a brief overview of the literature concerning CFS columns. Shanmugam and Dhanalakshmi (2001) [2] examined the influence of the web plate slenderness ratio and opening area ratio on the ultimate compressive strengths of perforated CFS channel stub columns. Moen and Schafer (2007) [3] found that the presence of slotted holes in CFS columns affected the post-peak response and ductility, influenced by the column's cross-section type and length. Yao and Rasmussen (2012) [4] explored the effects of perforations on inelastic stress distributions, load transfers, and failure modes of perforated simply supported plates and C-section columns. They observed distinct failure modes and stress distribution changes due to perforations. Kulatunga and Macdonald (2013) [5] investigated the influence of perforation positions, while Kulatunga et al. (2014) [6] studied the effect of perforation shapes on the ultimate compressive strengths of CFS columns with lipped channel cross-sections. Singh et al. [7] experimentally studied the axial compressive capacity of CFS square hollow-section (SHS) and rectangular hollow-section (RHS) columns containing circular perforations, noting conservative but generally scattered predictions by existing design equations. Additionally, various studies investigated the compression behaviour of columns under geometrical imperfections using design methodologies such as the direct strength method (DSM) [8] and continuous strength method (CSM) [9], and design codes such as Eurocode 3 (EC3) and Eurocode 9 (EC9).

Limited research has been conducted on the compressive capacity of aluminium columns, with most existing studies concentrating on SHS, RHS, and circular hollow sections (CHSs) [10–12]. Zhu and Young [13–15] conducted finite element (FE) investigations on various aluminium alloy hollow sections (SHS, RHS, and CHS), both welded and non-welded, focusing on their axial compressive capacity. They developed tailored design equations for aluminium alloy tubes with transverse welds at column ends. Zhou and Young [16] also examined the effect of circular holes on the web crippling strength of aluminium alloy SHSs through experimental and numerical analyses. Mohandas et al. [17] explored the axial compressive capacity of SHS stub columns made from aluminium alloy, finding that those constructed from 6061-T6 grade aluminium exhibit promising structural behaviour as a potential substitute for steel stub columns. Su et al. [18] conducted an experimental study on aluminium alloy SHS and RHS columns to examine their cross-section capacity and to explore the potential leverage of strain hardening in design, with and without internal cross stiffeners. Later, Su et al. [19] investigated the influence of strain hardening and moment redistribution on the compressive behaviour and design of aluminium alloy structures. Using the CSM, they analysed approximately 900 experimental and numerical results. Their findings indicate that CSM yields more accurate mean resistance predictions and reduces variability for both determinate and indeterminate aluminium alloy structures, in comparison to the Aluminum Design Manual [20], the Australian/New Zealand Standard [21], and Eurocode 9 [22]. Additionally, Feng et al. [23] and Feng and Liu [24] studied the flexural buckling performance of 6061-T6 and 6063-T5 normal-strength SHS and RHS columns with circular openings, comparing experimental and numerical findings with current standards. Furthermore, various column shapes, including RHS [25], SHS [26], CHS [15,27], angle-sections [28,29], I-sections [30–32], and others [33–35], were investigated. The analysis revealed that existing standards generally

offered inaccurate predictions of resistance for columns failing due to flexural buckling, local buckling, torsional buckling, or combined buckling.

In the manufacturing of aluminium columns, advancements in additive manufacturing complement the traditional extrusion process used for producing aluminium profiles. These developments facilitate the creation of complex geometrical structures, including relatively short columns optimised through topology optimisation. A notable example is the recent use of topology optimisation in designing additively manufactured joints for cylindrical gridshell structures. Zuo et al. (2023) [36] established a parametric workflow for optimising the topology and additive manufacturing of steel joints in gridshells, employing the bi-directional evolutionary structural optimisation (BESO) algorithm to enhance structural performance across various design parameters.

This study draws upon the previous work by Tsavdaridis et al. [37,38], which resulted in a series of highly optimised cross-sections tailored for aluminium columns, with a prime objective of augmenting their performance. Given aluminium's lower stiffness relative to steel, conventional structural elements may necessitate optimisation of their cross-sections to enhance structural efficacy. While certain aluminium alloys, like AL 6061-T6, boast yield and ultimate strength akin to or surpassing those of common structural steels, their inferior stiffness underscores the need for cross-sectional optimisation strategies.

While there are several studies focusing on individual optimised aluminium cross-section types, there is a significant gap in comprehensive research that compares multiple optimised designs under varying global and local imperfections. The existing literature does not widely explore the application of various design methods (CSM, DSM, and EC9) in this context, thereby creating a unique research opportunity for this study.

Expanding upon the original work by Tsavdaridis et al. [37], who introduced 16 innovative aluminium section beam and column profiles, this study advances the investigation. Marinopoulou et al. [38] utilised finite element analysis (FEA) with ABAQUS software to determine the ultimate compressive resistance values for stub columns, aligning FEA outcomes with those derived from CSM, DSM, and EC9 methodologies. With a focus on pin-ended columns featuring topology-optimised cross-sections, this research builds upon the modelling approach outlined in Georgantzia et al.'s [39] study, which explored the compressive behaviour of C-section aluminium columns. This study extends its scope to encompass stub and pin-end columns, with the FEA model of pin-ended aluminium columns validated against Georgantzia et al.'s findings. Following experiment validation, a parametric inquiry delves into both standard and novel cross-sections, assessing the efficacy of modern design techniques. Therefore, the primary aim of this study is to conduct a comprehensive comparison of 16 different optimised aluminium cross-section types across two different column lengths, each subject to three different global imperfections and corresponding local imperfections, utilising the CSM, DSM, and EC9 as design frameworks. A total of 288 distinct FEA models are created and analysed to determine the maximum load capacity of these columns.

The structure of the paper is as follows: Section 2 outlines the geometrical representation, followed by the FEA model given in Section 3. Section 4 provides a comparison of the FEA models against the experiments conducted by [39,40]. Section 5 details the modern design methodologies for assessing buckling loads. The parametric investigation is given in Section 6, followed by the findings and their discussion in Section 7. Section 8 outlines the conclusions drawn from this study.

2. Geometrical Representation

In this study, the novel cross-sections examined by Marinopoulou et al. [38] were utilised with slight adjustments. Square hollow sections (SHSs) featuring both inner and outer fillets have been included, as they offer better manufacturability compared to profiles without radii or with radii only on the inner or outer edges. The incorporation of corner radii enhances the effectiveness of extrusion manufacturing processes. Imperfection parameters are sourced from Georgantzia et al. [39], and the various types of cross-sections

are illustrated in Figures 1 and 2. Detailed cross-sectional dimensions are provided in Table 1.

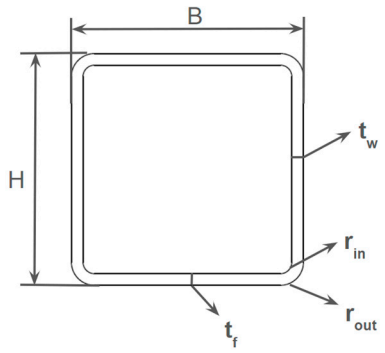

Figure 1. The generic representation of square hollow sections used in analyses.

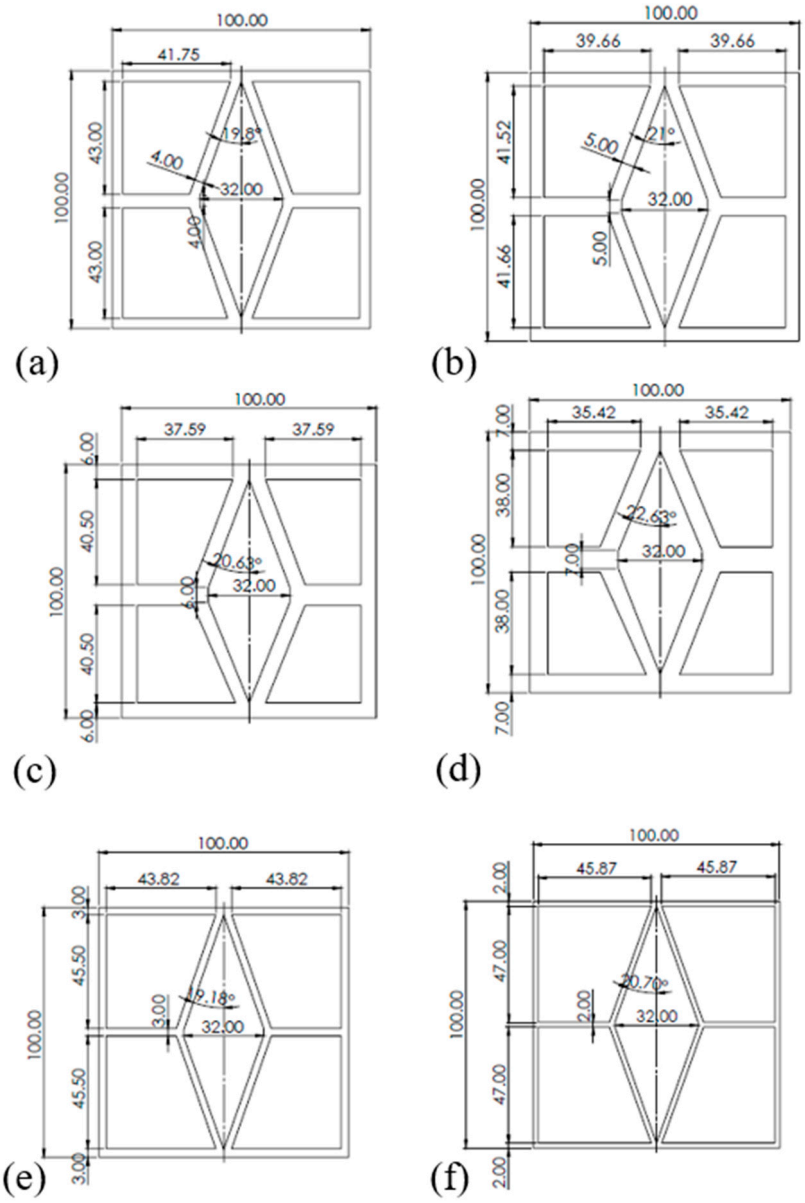

Figure 2. Novel cross-section geometries with the section codes N1-N6 have been assigned for these cross-sections: (**a**) N1, (**b**) N2, (**c**) N3, (**d**) N4, (**e**) N5, (**f**) N6.

Table 1. Cross-section dimensions.

Cross-Section Codes	B (mm)	H (mm)	t-Wall (mm)	t-Flange (mm)	Inner Filet (mm)	Outer Filet (mm)
A1	100	100	5	5	-	-
A2	100	100	7	7	-	-
A3	100	100	7	5	-	-
A4	100	100	5	7	-	-
A5	100	100	3	3	-	-
B1	100	100	7	7	8	15
B2	100	100	7	7	13	20
B3	100	100	7	7	23	30
B4	100	100	7	7	28	35
B5	100	100	3	3	7	10
N1	100	100	4	4	-	-
N2	100	100	5	5	-	-
N3	100	100	6	6	-	-
N4	100	100	7	7	-	-
N5	100	100	3	3	-	-
N6	100	100	2	2	-	-

3. Finite Element Analysis (FEA) Model

Columns inherently possess geometric imperfections due to manufacturing processes and other external factors. Aluminium columns tend to be more imperfect than steel columns due to the nature of aluminium. Aluminium has a smaller elastic modulus and it deforms easily. These factors result in higher imperfection values for aluminium columns after its production, especially for thin sections. Moreover, aluminium alloys are more ductile than steel and its alloys, and plastic deformations occur during manufacturing. In the FEA model, geometric imperfections are incorporated by introducing predefined imperfections based on the first mode of buckling. To incorporate these imperfections into the FEA, a two-step approach is adopted, comprising eigenvalue buckling analysis in advance of the nonlinear static analysis in ABAQUS. The eigenvalue buckling analysis is employed to determine the imperfect shapes of the columns, which are subsequently factored and integrated before being utilised as the initial conditions for the nonlinear static analysis.

The FEA model incorporates two types of geometric imperfections: global and local imperfections. Initial conditions for the static analysis are determined using the first global and local eigen buckling modes, which are then adjusted using imperfection factors. These factors are dependent on column dimensions such as effective length, wall thickness, and flange thickness. Specifically, the global imperfection factor is set at $L/1000$, where L represents the column length, while the local imperfection factor is defined as $t_f/15$, with t_f representing the flange thickness of the column cross-section. Similar parameter values as those used in [39] were employed here as they encompass typical configurations of aluminium columns.

The aluminium C-section column is represented using shell elements, depicted in Figure 3. Utilising shell elements is a widely adopted practice for thin-walled columns, as demonstrated in the literature [8,10,12,39]. S4R element from the ABAQUS element library was employed. To simulate the pin-ended column test accurately, one of the rotational degrees of freedom is left unconstrained. This is achieved using KINEMATIC COUPLING constraints via the RBE2 element, as illustrated in Figure 4, since both ends of the column are pin-ended. Specifically, the UX and ROTY degrees of freedom (DOFs) are set free based on the column's orientation during the column test.

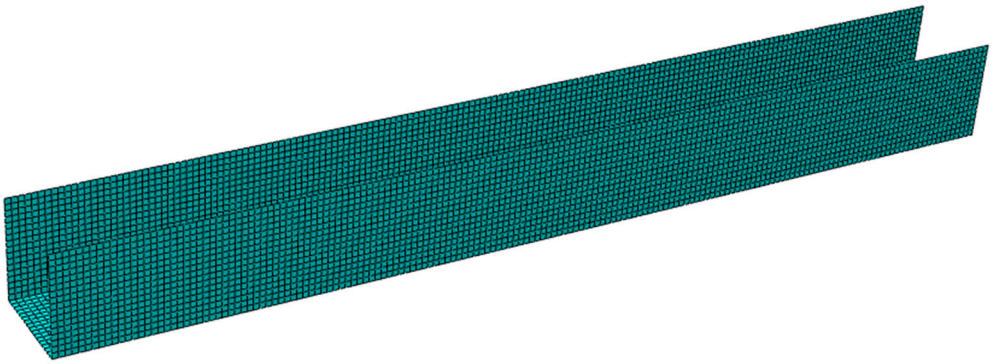

Figure 3. FEA model for 50.8 × 50.8 × 6.35-L500 specimen in Ref. [39].

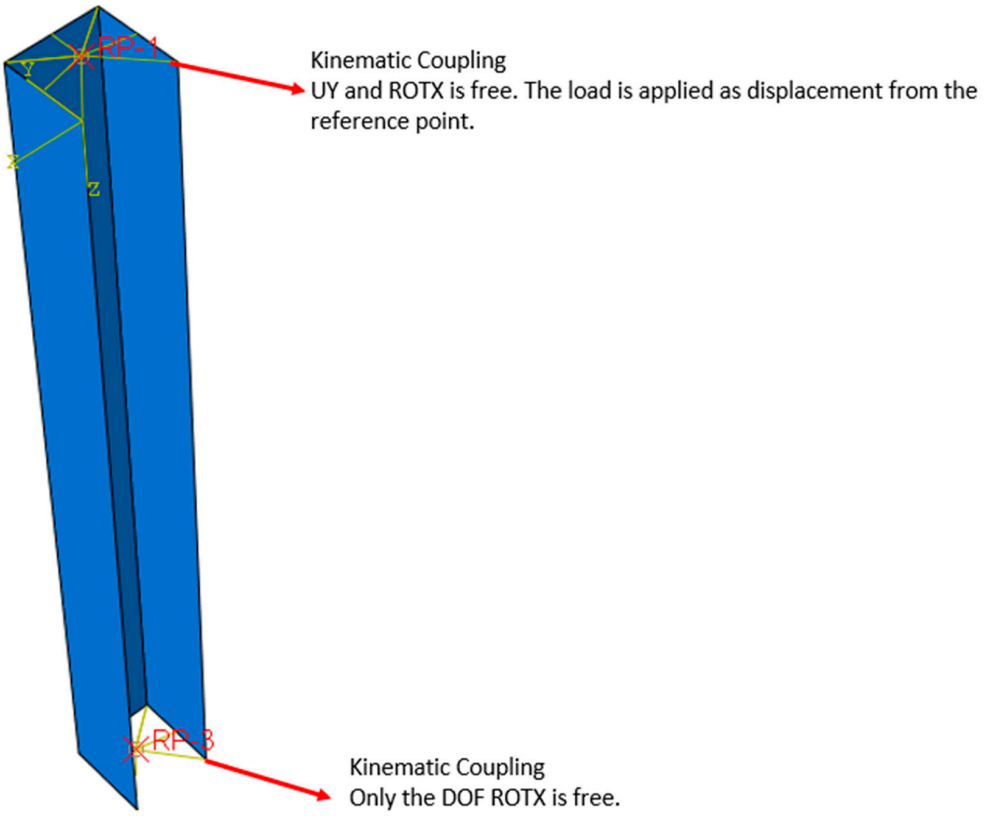

Figure 4. Boundary conditions of the validation FEA model for 50.8 × 50.8 × 6.35-L500 specimen in Ref. [39].

Mesh convergence studies were conducted to optimise computational efficiency. A column with a square hollow section measuring 100 mm × 100 mm × 5 mm and extending 1 m in length was modelled using four different mesh sizes ranging from 2 mm to 5 mm. After comparing the results, it was found that the buckling load value varied within approximately ±1%. Consequently, a mesh size of 5 mm was selected for all simulations to improve computational efficiency. Considering the substantial number of simulation cases—totalling 288—that must be addressed, computational efficiency is a crucial aspect of this study.

In the parametric studies, a bilinear hardening model was employed due to the limited tangent modulus of AL6063-T6. In the bilinear material model, the tangent modulus is determined based on a yield stress of 160 MPa, an ultimate stress of 193 MPa, and an elongation of 0.106, all obtained from EC9 [22].

4. Comparisons with Experiments

Georgantzia et al. [39] conducted both experimental and numerical investigations on C-section columns made from 6082-T6 heat-treated aluminium alloy. In this paper, the FEA models were validated against the experimental results of Refs. [39,40]. In the validation studies, a multilinear hardening material model was adopted.

The comparison between the maximum load and mid-height deflection results of the first validation study is depicted in Figure 5, showing an exceptional alignment between the outcomes. Specifically, Table 2 provides a detailed comparison of the ultimate load between the findings of [39] and those derived from the present investigation.

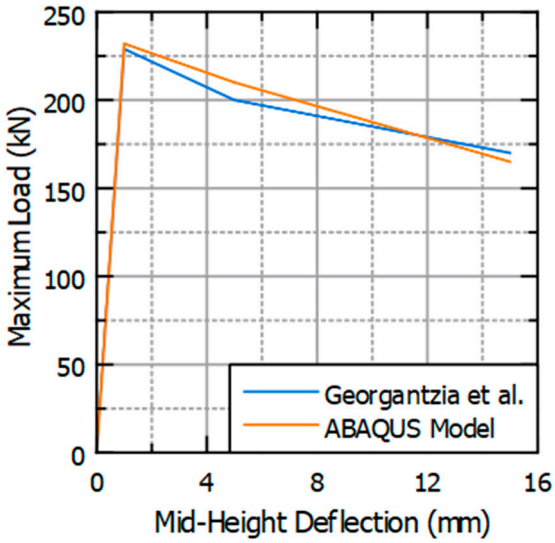

Figure 5. Comparison of the FEA result with the experimental result of Georgantzia et al. [39] for the column with dimensions 50.8 × 50.8 × 6.35-L500.

Table 2. Results of Georgantzia et al. [39] and ABAQUS model.

Results		Ultimate Load (kN)
Georgantzia et al. [39]	2023-Test	225.9
Georgantzia et al. [39]	2023-FEM	229.0
FEA-ABAQUS		231.0

Chen et al. [40] also investigated the compressive behaviour of aluminium columns to develop design methods. H-section columns made of AL6061 T6 were used for the second validation. In this validation study, mesh size, material properties, and imperfections were adopted from Chen et al. [40] (see Figure 6 for the FEA model used). The same boundary conditions from the first validation study were directly applied to the model. A comparison of the experimental results from [40] with the FEA results is given in Figure 7, which shows a 2.4% difference in maximum load, demonstrating the reliability of the FEA methodology used in this study.

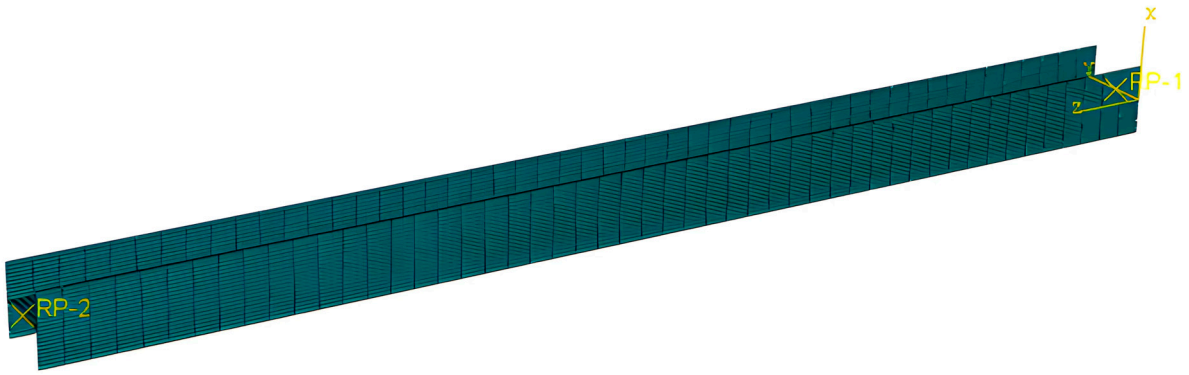

Figure 6. FEA model for the C6061-80 × 80 × 1350 specimen in Ref. [40].

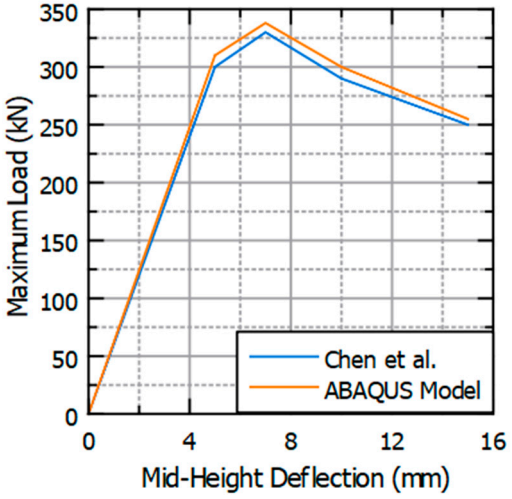

Figure 7. Comparison of the FEA result with the experimental result of Chen et al. [40] for the C6061-80 × 80 × 1350 specimen.

5. Modern Design Methodologies for Assessing Buckling Loads

Modern design methods are empirically derived and standardised approaches used by engineers in their design processes. In both validation and parametric studies, methods such as the direct strength method (DSM), continuous strength method (CSM), and EC9 were utilised. Although these methods are traditionally designed for standard cross-sections like square hollow sections and circular hollow sections, this study emphasises their application to novel cross-sections rather than conventional ones. A brief overview of these methods is provided herein.

5.1. Direct Strength Method (DSM)

Schafer and Peköz [41] pioneered the DSM for cold-formed steel structures, leveraging data from concentrically loaded pin-ended cold-formed steel columns [42,43]. Subsequently, Zhu and Young [13–15,44] adapted DSM, with certain adjustments, for designing aluminium alloy SHS and RHS columns. This approach initially computes the non-dimensional slenderness for flexural buckling, denoted as λ_c, using the following formula:

$$\lambda_c = \sqrt{P_y / P_{cre}} \tag{1}$$

where P_{cre} represents the Euler critical elastic buckling load and P_y signifies the yield load:

$$P_{cre} = \frac{\pi^2 EA}{\left(l_{eff}/r\right)^2} \tag{2}$$

$$P_y = \sigma_y \cdot A \tag{3}$$

Next, the nominal axial load for flexural buckling, P_{ne}, is calculated from:

$$P_{ne} = \begin{cases} \left(0.658^{\lambda_c^2}\right) \cdot P_y \text{ for } \lambda_c \leq 1.5 \\ \left(\frac{0.877}{\lambda_c^2}\right) \cdot P_y \text{ for } \lambda_c \geq 1.5 \end{cases} \tag{4}$$

Furthermore, P_{crl} represents the limit state load for the cross-section, which can be calculated using the following formula [45]:

$$P_{crl} = A \cdot \sigma_{crl} = A \cdot k \frac{\pi^2 E}{12(1-\nu^2)} \left(\frac{t}{b}\right)^2 \tag{5}$$

The non-dimensional slenderness for the interaction of local and flexural buckling, denoted as λ_l, is then calculated using:

$$\lambda_l = \sqrt{P_{ne} / P_{crl}} \tag{6}$$

Using the value of λ_l, the nominal axial strength for local buckling, P_{nl}, can be calculated from:

$$P_{nl} = \begin{cases} \left(0.658^{\lambda_c^2}\right) \cdot P_{ne}, & \lambda_l \leq 0.713 \\ \left[1 - 0.15 \cdot \left(\frac{P_{crl}}{P_{ne}}\right)^{0.3}\right] \cdot \left(\frac{P_{crl}}{P_{ne}}\right)^{0.3}, & \lambda_l > 0.713 \end{cases} \tag{7}$$

Finally, the DSM limit load can be found from the minimum of (P_{ne}, P_{nl}) given in Equations (4) and (7).

5.2. Continuous Strength Method (CSM)

Originally designed for stainless steel and carbon steel materials, CSM is a deformation-based design framework that incorporates the advantageous effects of strain hardening. A series of studies in the literature [46–50] have been undertaken to develop and refine the CSM for CFS structures. Su et al. [19] modified this approach to be used for aluminium alloy structural elements.

The approach emphasises the deformation capacity of the cross-section, deriving it from a material curve that incorporates both linear and nonlinear components. Unlike DSM and Eurocode, the CSM evaluates strain rather than stress, distinguishing its methodology. In this method, first, critical buckling stress, σ_{cr}, is calculated using the following:

$$\sigma_{cr} = k \frac{\pi^2 E}{12(1-\nu^2)} \left(\frac{t}{b}\right)^2 \tag{8}$$

Then, cross-sectional slenderness, λ_p, is calculated

$$\lambda_p = \sqrt{\sigma_y / \sigma_{cr}} \tag{9}$$

For stocky $(\lambda_p \leq 0.68)$ and slender $(\lambda_p > 0.68)$ cross-sections, CSM strain, ε_{csm}, can be found from the following relation:

$$\frac{\varepsilon_{csm}}{\varepsilon_y} = \begin{cases} \frac{0.25}{\lambda_p^{3.6}} & \lambda_p \leq 0.68 \\ \left(1 - \frac{0.222}{\lambda_p^{1.05}}\right) \cdot \frac{1}{\lambda_p^{1.05}} & \lambda_p > 0.68 \end{cases} \tag{10}$$

Thus, the limit stress can be calculated from:

$$\sigma_{csm} = \sigma_y + E_t\left(\varepsilon_{csm} - \varepsilon_y\right) \tag{11}$$

where E_t is the tangent modulus of the nonlinear part of the stress–strain curve and ε_y is the yield strain.

5.3. Eurocode 9 (EC9)

According to EC9, the material buckling class for 6063-T6 aluminium material is "Class A". The limit buckling load is given as:

$$N_{b,Rd} = \kappa \chi A f_0 / \gamma_{M1} \tag{12}$$

where

$$\chi = \frac{1}{\phi + \sqrt{\phi^2 - \bar{\lambda}^2}} \text{ but } \chi \leq 1.0 \tag{13}$$

$$\phi = 0.5\left(1 + \alpha\left(\bar{\lambda} - \bar{\lambda}_0\right) + \bar{\lambda}^2\right) \tag{14}$$

and f_0 is the yield stress. Note that for material class A, $\alpha = 0.2$ and $\bar{\lambda}_0 = 0.1$. The slenderness $\bar{\lambda}$ is defined as:

$$\bar{\lambda} = \sqrt{\frac{A f_o}{N_{cr}}} \tag{15}$$

where N_{cr} is the elastic critical force for the relevant buckling mode based on the gross cross-sectional properties.

5.4. Comparison of FEA Results with Those of the Design Codes

Maximum load calculated using the aluminium column FEA model simulated with ABAQUS FE Static RIKS Solver was compared with all three methods explained above. The results summary is presented in Table 3.

Table 3. Maximum load results comparison between [39] and each calculation method.

Test	Paper-FEM	FEM	EC9	DSM	CSM
226 kN	229 kN	231 kN	203.5 kN	212.4 kN	231 kN
Ratio = This study/Ref. [39]	1.014	1.022	0.901	0.939	1.022

6. Parametric Study

Table 4 and Figure 8 present the comprehensive conditions encompassing cross-section types, imperfection specifications, and column lengths considered in this study. Each cross-section variant is tested across both column lengths. Also, for each length, three of the global imperfections have been applied to columns. For each global imperfection value, three of the local imperfections have been combined for the study. Subsequently, all specified local imperfection values are individually applied to each setup. Global imperfection values are determined based on the effective length of the column, while local imperfection values are calculated using the flange thickness.

For considering imperfections, the same approach as used earlier in the validation study is followed. To ensure mesh convergence, column A1 is simulated with four different mesh sizes ranging from 2 mm to 5 mm. Upon comparison, the buckling load values exhibit a variation of approximately ±1%. Consequently, to optimise computational efficiency, a mesh size of 5 mm is selected for all simulations. Given the substantial number of simulation cases, computational efficiency is a paramount concern in this study.

A bilinear plasticity material model was adopted, as it is well suited for this analysis due to the material's minimal tangent modulus. While aluminium shows nonlinear hardening, this simplified model provides accurate results for the study's focus on buckling and ultimate load capacity, and aligns with previous studies for comparison purposes. The model employs a 5 mm free mesh utilising S4R elements in ABAQUS. Boundary

conditions are applied from both ends of the column, with a centre node coupled using KINEMATIC COUPLING.

Table 4. Cases of analyses.

Cross-Sections	Column Length 1 (mm)	Column Length 2 (mm)	Global Imperfection-1	Global Imperfection-2	Global Imperfection-3	Local Imperfection-1	Local Imperfection-2	Local Imperfection-3
A1	500	1000	Le/1000	Le/1500	Le/2000	tf/15	tf/50	tf/100
A2	500	1000	Le/1000	Le/1500	Le/2000	tf/15	tf/50	tf/100
A3	500	1000	Le/1000	Le/1500	Le/2000	tf/15	tf/50	tf/100
A4	500	1000	Le/1000	Le/1500	Le/2000	tf/15	tf/50	tf/100
A5	500	1000	Le/1000	Le/1500	Le/2000	tf/15	tf/50	tf/100
B1	500	1000	Le/1000	Le/1500	Le/2000	tf/15	tf/50	tf/100
B2	500	1000	Le/1000	Le/1500	Le/2000	tf/15	tf/50	tf/100
B3	500	1000	Le/1000	Le/1500	Le/2000	tf/15	tf/50	tf/100
B4	500	1000	Le/1000	Le/1500	Le/2000	tf/15	tf/50	tf/100
B5	500	1000	Le/1000	Le/1500	Le/2000	tf/15	tf/50	tf/100
N1	500	1000	Le/1000	Le/1500	Le/2000	tf/15	tf/50	tf/100
N2	500	1000	Le/1000	Le/1500	Le/2000	tf/15	tf/50	tf/100
N3	500	1000	Le/1000	Le/1500	Le/2000	tf/15	tf/50	tf/100
N4	500	1000	Le/1000	Le/1500	Le/2000	tf/15	tf/50	tf/100
N5	500	1000	Le/1000	Le/1500	Le/2000	tf/15	tf/50	tf/100
N6	500	1000	Le/1000	Le/1500	Le/2000	tf/15	tf/50	tf/100

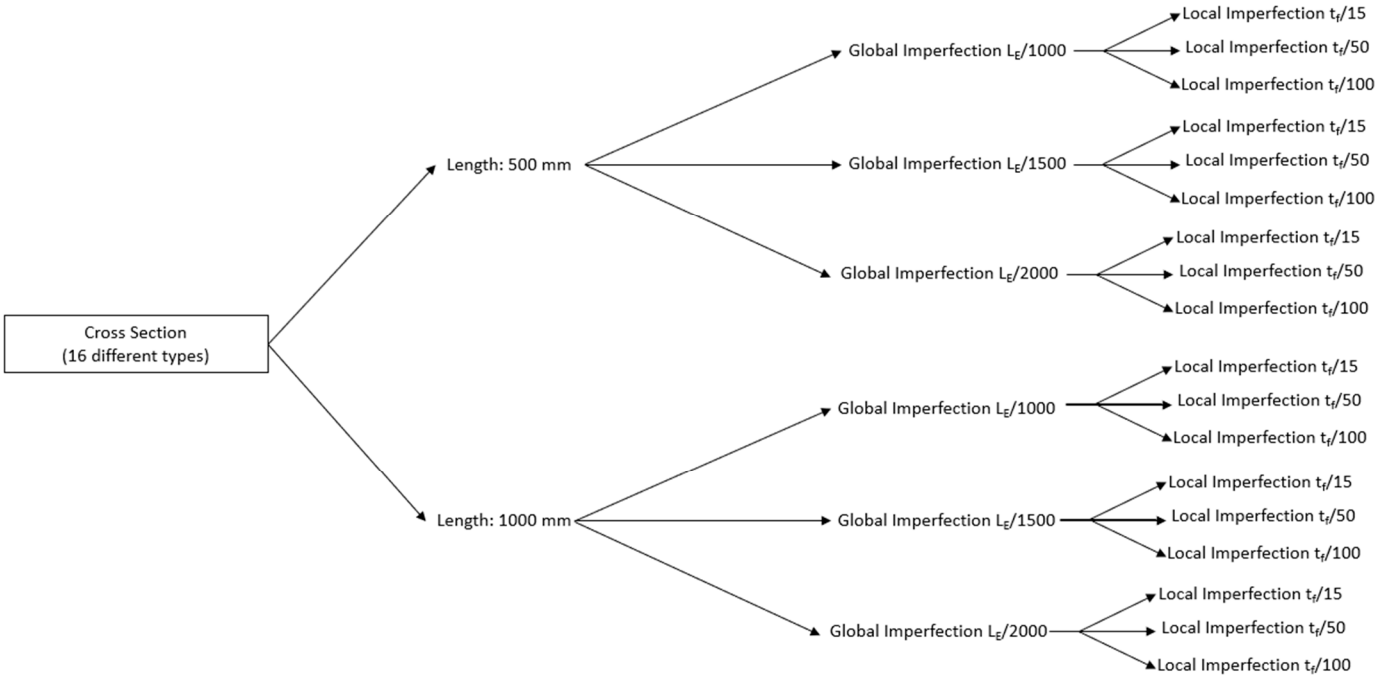

Figure 8. Roadmap of FEM studies for a column.

7. Results and Discussion

A set of 288 finite element models were used to assess the impact of imperfection values. Across all cases, there exists an average deviation of 3% between the lowest and highest imperfection values, with a maximum deviation of 5.4%. Given that the first global mode has been applied as the global imperfection factor, columns exhibit a half-sine wave shape upon buckling. Notably, the alteration of local factors yields a minimal impact on the results, with variations less than 1% observed across all models.

Figure 9 portrays the behaviour exhibited by the columns, demonstrating a global buckling pattern with observable deformations on the walls and flanges induced by local imperfections. This underscores the predominant influence of global imperfections on the failure behaviour, attributed to the manufacturing process. In instances where columns have shorter lengths, the behaviour aligns with the first mode of global imperfection, leading to failure primarily at the walls and/or flanges. Conversely, longer columns exhibit a half-sine deflection along their length, indicative of Euler failure mode dependence.

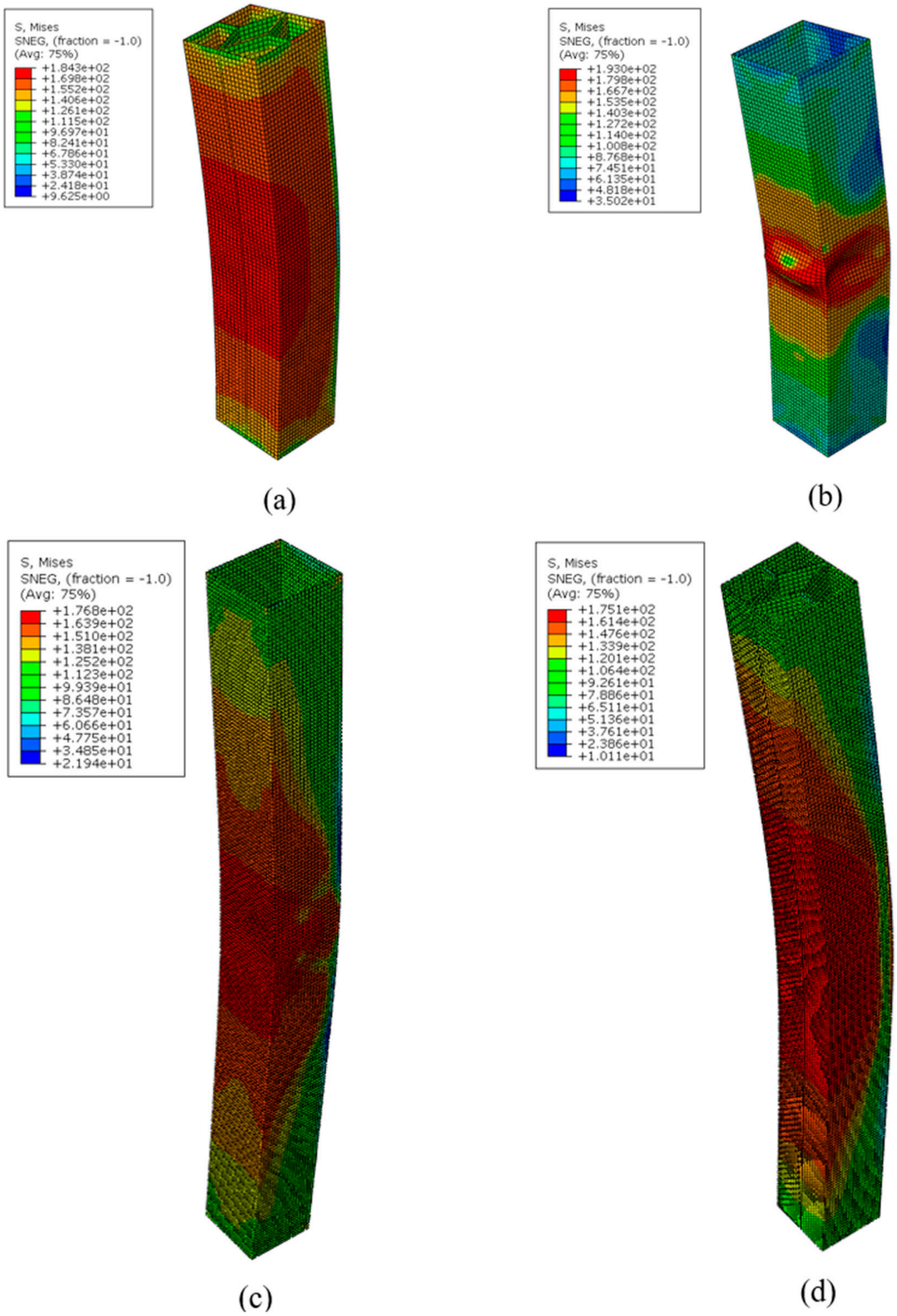

Figure 9. Some examples of buckling results of various columns with equivalent stress contours (MPa) (**a**) N2-0.5 m, (**b**) B1-0.5 m, (**c**) N4-1 m, (**d**) A4-1 m.

In the comparative analysis, the finite element results for each column are averaged across all imperfection scenarios. Table 5 provides a comparison between the results obtained from FE modelling and calculations based on EC9. It is observed that the disparity between FEM and EC9 calculations increases with the slenderness value, with EC9 values consistently surpassing FEM results.

Table 5. FEM results and EC-9 results.

Cross-Section Code	Length (m)	FEM-Average (kN)	EC-9 (kN)	FEM/EC9
A1	0.5	318.1	358.9	0.89
A1	1	313.5	337.2	0.93
A2	0.5	445.7	491.4	0.91
A2	1	439	460.8	0.95
A3	0.5	382.1	425.8	0.90
A3	1	376.7	398.3	0.95
A4	0.5	382	427.5	0.89
A4	1	375.8	402.4	0.93
A5	0.5	189.8	220.1	0.86
A5	1	185.8	207.2	0.90
B1	0.5	416.7	464.5	0.90
B1	1	409.9	435.2	0.94
B2	0.5	406.6	453.2	0.90
B2	1	402.5	423.8	0.95
B3	0.5	387.5	430	0.90
B3	1	380.4	400.9	0.95
B4	0.5	377.8	418	0.90
B4	1	371.6	389.2	0.95
B5	0.5	182	211.7	0.86
B5	1	179.2	199.1	0.90
N1	0.5	429.8	492.8	0.87
N1	1	420.5	455.4	0.92
N2	0.5	532.4	577.7	0.92
N2	1	521.5	531.4	0.98
N3	0.5	626.1	706.2	0.89
N3	1	613	651.8	0.94
N4	0.5	747.3	759.3	0.98
N4	1	612.9	699.9	0.88
N5	0.5	308.9	365	0.85
N5	1	301.9	338.5	0.89
N6	0.5	208	246.1	0.85
N6	1	201.2	228.5	0.88
Mean				0.91
COV				0.04

Table 6 presents the results of the direct strength method (DSM) alongside their comparison with FEM results. Across all cases, FEM results are higher than those obtained from DSM, albeit with less sensitivity to slenderness compared to EC9.

Table 7 offers a comparison between FEM results and those derived from the continuous strength method (CSM). Notably, this comparison yields lower error values, with FEM results generally exceeding those of CSM. However, this trend shifts within certain slenderness ratios (0.32–0.43).

Figures 10 and 11 present the comparison results based on slenderness values outlined in the preceding section. DSM exhibits precision for slenderness values below 0.4, while EC9 yields satisfactory results for slenderness values exceeding 0.22. CSM generally outperforms other methods, consistent with findings in the literature. Notably, CSM results exhibit the lowest coefficient of variation (COV), indicating superior precision. By directly calculating cross-sectional strength with plasticity correction, CSM offers adequate results without requiring significant modifications.

Table 6. FEM results and DSM results.

Cross-Section Code	Length (m)	FEM-Average (kN)	DSM (kN)	FEM/DSM
A1	0.5	318.1	294.4	1.08
A1	1	313.5	267.4	1.17
A2	0.5	445.7	403	1.11
A2	1	439	364.6	1.2
A3	0.5	382.1	349.1	1.09
A3	1	376.7	314.1	1.2
A4	0.5	382	350.7	1.09
A4	1	375.8	319.8	1.18
A5	0.5	189.8	180.6	1.05
A5	1	185.8	164.6	1.13
B1	0.5	416.7	381.1	1.09
B1	1	409.9	343.5	1.19
B2	0.5	406.6	371.6	1.09
B2	1	402.5	334.1	1.2
B3	0.5	387.5	352.3	1.1
B3	1	380.4	314.9	1.21
B4	0.5	377.8	342.5	1.1
B4	1	371.6	305	1.22
B5	0.5	182	173.6	1.05
B5	1	179.2	157.9	1.13
N1	0.5	429.8	403.3	1.07
N1	1	420.5	353.7	1.19
N2	0.5	532.4	472.4	1.13
N2	1	521.5	410.4	1.27
N3	0.5	626.1	577.8	1.08
N3	1	613	505.4	1.21
N4	0.5	747.3	621	1.2
N4	1	612.9	542.2	1.13
N5	0.5	308.9	298.9	1.03
N5	1	301.9	264	1.14
N6	0.5	208	201.6	1.03
N6	1	201.2	178.5	1.13
Mean				1.13
COV				0.06

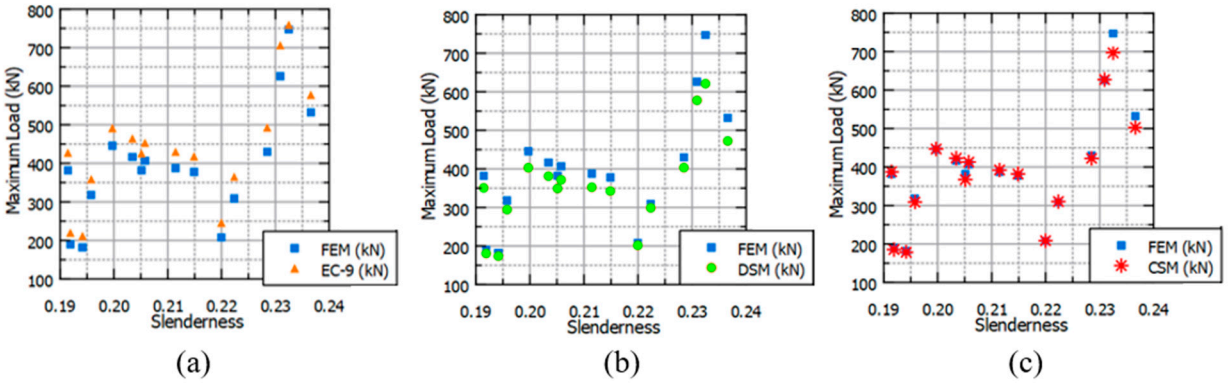

Figure 10. Methods comparison with respect to FEM results of 0.5 m columns (**a**): FEM vs. EC-9, (**b**): FEM vs. DSM, (**c**): FEM vs. CSM.

Table 7. FEM results and CSM results.

Cross-Section Code	Length (m)	FEM-Average (kN)	CSM (kN)	FEM/CSM
A1	0.5	318.1	308.8	1.03
A1	1	313.5	308.8	1.015
A2	0.5	445.7	446.9	0.997
A2	1	439	446.9	0.982
A3	0.5	382.1	367.4	1.04
A3	1	376.7	367.4	1.025
A4	0.5	382	387.8	0.985
A4	1	375.8	387.8	0.969
A5	0.5	189.8	185.4	1.024
A5	1	185.8	185.4	1.002
B1	0.5	416.7	423.2	0.985
B1	1	409.9	423.2	0.969
B2	0.5	406.6	412.9	0.985
B2	1	402.5	412.9	0.975
B3	0.5	387.5	392.3	0.988
B3	1	380.4	392.3	0.97
B4	0.5	377.8	381.8	0.99
B4	1	371.6	381.8	0.973
B5	0.5	182	178.4	1.02
B5	1	179.2	178.4	1.004
N1	0.5	429.8	422.4	1.018
N1	1	420.5	422.4	0.996
N2	0.5	532.4	502.9	1.059
N2	1	521.5	502.9	1.037
N3	0.5	626.1	627.2	0.998
N3	1	613	627.2	0.977
N4	0.5	747.3	696.9	1.072
N4	1	612.9	696.9	0.879
N5	0.5	308.9	310.2	0.996
N5	1	301.9	310.2	0.973
N6	0.5	208	208.4	0.998
N6	1	201.2	208.4	0.965
Mean				0.99
COV				0.03

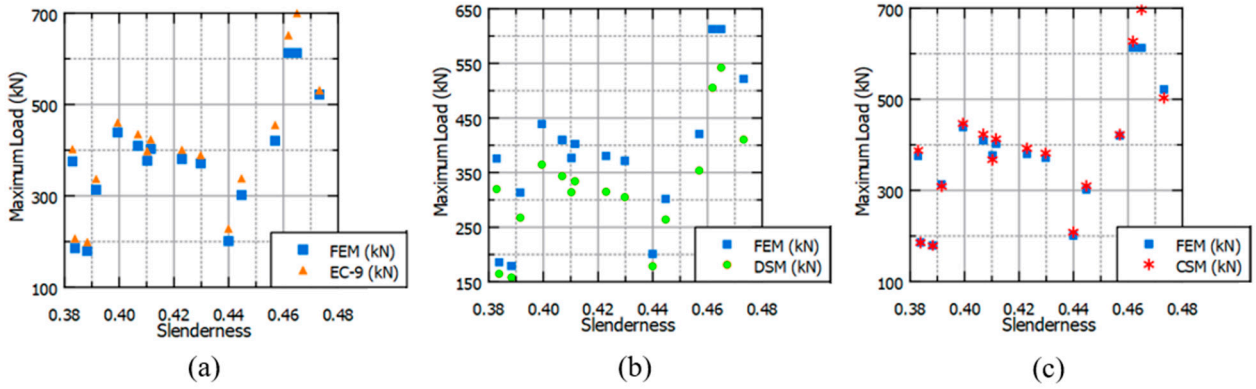

Figure 11. Methods comparison with respect to FEM results of 1 m columns (**a**): FEM vs. EC-9, (**b**): FEM vs. DSM, (**c**): FEM vs. CSM.

Figure 12 provides the precision of methods with respect to slenderness values. As mentioned before, CSM methods work perfectly with all slenderness values. EC9 works better for slenderness values between 0.4 and 0.43; however it may need some improvement, especially for other slenderness values. On the other hand, DSM works better for

slenderness values between 0.2 and 0.215, but it also needs some improvement. For other slenderness values, it has divergent characteristics.

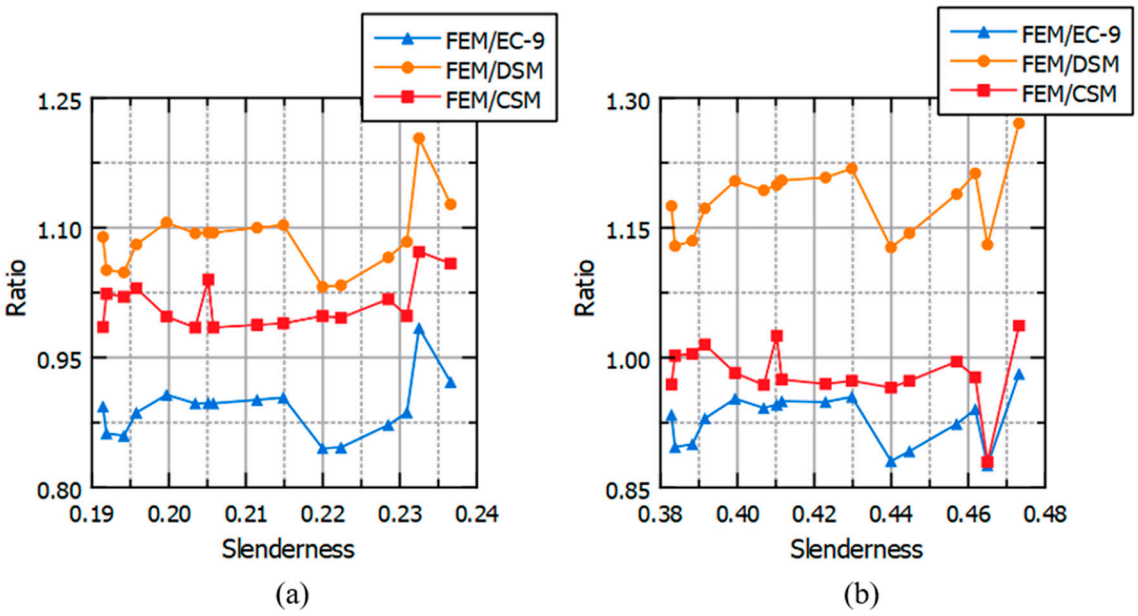

Figure 12. Change in load ratios with slenderness (**a**): 0.5 m columns (**b**): 1 m columns.

The nonlinear relationship between maximum load and slenderness values primarily stems from variations in cross-sectional inertia across different slenderness values. Since slenderness values encompass three distinct geometries, each with varying inertia-to-cross-sectional-area ratios, this variability contributes to the observed nonlinearity in results. Additionally, differences in local imperfection modes across various cross-sectional types influence both maximum load and column failure mode.

8. Concluding Remarks

This paper presents a numerical investigation of novel aluminium alloy sections using finite element analysis (FEA). The FEA models incorporate geometric imperfections and material nonlinearity, with validation against experimental results from the literature. An extensive parametric analysis was conducted on 288 models featuring different cross-sections, column lengths, and global and local imperfections. The FEA results were compared with modern design approaches such as Eurocode 9, the direct strength method, and the continuous strength method. From the results of this study, the following conclusions can be drawn:

- The newly optimised aluminium columns outperform conventional cross-sections with only a minimal increase in mass, providing superior mass-to-ultimate-load efficiency.
- Traditional columns require larger cross-sections or additional compressive members, whereas these novel sections offer enhanced performance without compromising on weight.
- The study shows an average 3% deviation in ultimate compressive load between the smallest and largest global imperfection values, with a maximum deviation of 5.4%.
- Local imperfections had minimal impact on performance, with deviations less than 1% across all models, highlighting their limited influence on overall column stability.
- Shorter columns tend to fail at the walls or flanges, consistent with first-mode global imperfection buckling, while longer columns display a half-sine deflection indicative of Euler failure modes.
- EC9 calculations consistently overestimated the ultimate load compared to FEM results, with greater discrepancies observed at higher slenderness values.

- The continuous strength method (CSM) demonstrated the smallest errors and highest precision, particularly in directly calculating cross-sectional strength with adjustments for plasticity.
- A nonlinear relationship between maximum load and slenderness values was observed, influenced by variations in cross-sectional inertia and local imperfection modes across the different cross-section types.
- This study emphasises the importance of cross-sectional optimisation for efficient column design, especially where weight savings are critical without compromising load-bearing capacity.
- Future research could further refine these methods and explore their application to other structural materials or more complex geometries.

In summary, the comparison of EC9, DSM, and CSM provides valuable insights for the design of aluminium columns. While EC9 offers a conservative approach with well-established safety margins, DSM demonstrates flexibility in accounting for various imperfections. CSM, by considering material nonlinearity, proves to be more efficient for some optimised cross-sections. These findings suggest that CSM holds promise for enhanced performance in future design methods, though EC9 remains a reliable choice for conventional designs. This analysis points toward potential improvements in aluminium column design and further research opportunities.

Author Contributions: Conceptualization, M.A.G., A.A. and K.D.T.; Methodology, M.A.G. and A.A.; Software, A.A.; Validation, A.A. and M.A.G.; Formal Analysis, A.A. and M.A.G.; Investigation, M.A.G., A.A. and K.D.T.; Resources, A.A. and B.Y.; Data Curation, A.A.; Writing—Original Draft Preparation, M.A.G., A.A., B.Y. and K.D.T.; Writing—Review and Editing, M.A.G., A.A., B.Y. and K.D.T.; Visualization, A.A. and M.A.G.; Supervision, M.A.G. and K.D.T. All authors have read and agreed to the published version of the manuscript.

Funding: This research received no external funding.

Data Availability Statement: The original contributions presented in the study are included in the article, further inquiries can be directed to the corresponding author.

Conflicts of Interest: The authors declare no conflict of interest.

References

1. Georgantzia, E.; Gkantou, M.; Kamaris, G.S. Aluminium alloys as structural material: A review of research. *Eng. Struct.* **2021**, *227*, 111372. [CrossRef]
2. Shanmugam, N.E.; Dhanalakshmi, M. Design for openings in cold-formed steel channel stub columns. *Thin-Walled Struct.* **2001**, *39*, 961–981. [CrossRef]
3. Moen, C.D.; Schafer, B.W. Experiments on cold-formed steel columns with holes. *Thin-Walled Struct.* **2008**, *46*, 1164–1182. [CrossRef]
4. Yao, Z.; Rasmussen, K.J.R. Inelastic local buckling behaviour of perforated plates and sections under compression. *Thin-Walled Struct.* **2012**, *61*, 49–70. [CrossRef]
5. Kulatunga, M.P.; Macdonald, M. Investigation of cold-formed steel structural members with perforations of different arrangements subjected to compression loading. *Thin-Walled Struct.* **2013**, *67*, 78–87. [CrossRef]
6. Kulatunga, M.P.; Macdonald, M.; Rhodes, J.; Harrison, D.K. Load capacity of cold-formed column members of lipped channel cross-section with perforations subjected to compression loading—Part I: FE simulation and test results. *Thin-Walled Struct.* **2014**, *80*, 1–12. [CrossRef]
7. Singh, T.G.; Singh, K.D. Experimental investigation on performance of perforated cold-formed steel tubular stub columns. *Thin-Walled Struct.* **2018**, *131*, 107–121. [CrossRef]
8. Dong, D.; Fan, S.; Liu, M.; Zhu, T. Calculation method for local–global interaction buckling capacity of stainless steel C-columns. *Structures* **2023**, *58*, 105365. [CrossRef]
9. Yun, X.; Meng, X.; Gardner, L. Design of cold-formed steel SHS and RHS beam–columns considering the influence of steel grade. *Thin-Walled Struct.* **2022**, *171*, 108600. [CrossRef]
10. Ma, J.L.; Chan, T.M.; Young, B. Cold-formed high strength steel tubular beam-columns. *Eng. Struct.* **2021**, *230*, 111618. [CrossRef]
11. Chen, M.T.; Young, B. Material properties and structural behavior of coldformed steel elliptical hollow section stub columns. *Thin-Walled Struct.* **2019**, *134*, 111–126. [CrossRef]

12. Yun, X.; Gardner, L. The continuous strength method for the design of cold-formed steel non-slender tubular cross-sections. *Eng. Struct.* **2018**, *175*, 549–564. [CrossRef]
13. Zhu, J.H.; Young, B. Aluminum alloy tubular columns—Part I: Finite element modeling and test verification. *Thin-Walled Struct.* **2006**, *44*, 961–968. [CrossRef]
14. Zhu, J.H.; Young, B. Aluminum alloy tubular columns—Part II: Parametric study and design using direct strength method. *Thin-Walled Struct.* **2006**, *44*, 969–985. [CrossRef]
15. Zhu, J.H.; Young, B. Numerical investigation and design of aluminum alloy circular hollow section columns. *Thin-Walled Struct.* **2008**, *46*, 1437–1449. [CrossRef]
16. Zhou, F.; Young, B. Web crippling of aluminum tubes with perforated webs. *Eng. Struct.* **2010**, *32*, 1397–1410. [CrossRef]
17. Mohandas, M.; Joseph, B.M.; Sabu, N.V. Numerical investigation on aluminum alloy stub columns with openings. *Int. J. Innov. Res. Sci. Eng. Technol.* **2016**, *5*, 14944–14950.
18. Su, M.N.; Young, B. Testing and design of aluminum alloy cross-sections in compression. *J. Struct. Eng.* **2014**, *140*, 04014047. [CrossRef]
19. Su, M.N.; Young, B.; Gardner, L. The continuous strength method for the design of aluminum alloy structural elements. *Eng. Struct.* **2016**, *122*, 338–348. [CrossRef]
20. Aluminum Association (AA). *Aluminum Design Manual*; Aluminum Association (AA): Washington, DC, USA, 2010.
21. *AS/NZS 1664.1:1997*; Aluminum Structures Part 1: Limit State Design. Australian/New Zealand Standard (AS/NZS): Sydney, Australia, 1997.
22. *BS EN 1999-1-1:2007*; European Committee for Standardization (EC9). Eurocode 9: Design of Aluminium Structures—Part 1-1: General Rules—General Rules and Rules for Buildings. The European Committee for Standardization (CEN): Brussels, Belgium, 2007.
23. Feng, R.; Zhu, W.; Wan, H.Y.; Chen, A.Y.; Chen, Y. Tests of perforated aluminum alloy SHSs and RHSs under axial compression. *Thin-Walled Struct.* **2018**, *130*, 194–212. [CrossRef]
24. Feng, R.; Liu, J.R. Numerical investigation and design of perforated aluminum alloy SHS and RHS columns. *Eng. Struct.* **2019**, *199*, 109591. [CrossRef]
25. Hu, Y.; Rong, B.; Zhang, R.; Zhang, Y.; Zhang, S. Study of buckling behavior for 7A04-T6 aluminum alloy rectangular hollow columns. *Thin-Walled Struct.* **2021**, *169*, 108410. [CrossRef]
26. Li, B.; Wang, Y.; Zhang, Y.; Meng, X.; Yuan, H.; Zhi, X. Flexural buckling of extruded high-strength aluminum alloy SHS columns. *Thin-Walled Struct.* **2022**, *179*, 109717. [CrossRef]
27. Feng, R.; Mou, X.L.; Chen, Z.M.; Roy, K.; Chen, B.S. Finite-element modeling and design guidelines for axial compressive capacity of aluminum alloy circular hollow sections with holes. *Thin-Walled Struct.* **2020**, *157*, 107027. [CrossRef]
28. Zhang, Y.; Wang, Y.Q.; Wang, Z.X.; Bu, Y.D.; Fan, S.G. Experimental investigation and numerical analysis of pin-ended extruded aluminum alloy unequal angle columns. *Eng. Struct.* **2020**, *215*, 110694. [CrossRef]
29. Zhang, Y.; Bu, Y.D.; Wang, Y.Q.; Wang, Z.X.; Ouyang, Y.W. Study of flexural–torsional buckling behavior of 6061-T6 aluminum alloy unequal-leg angle columns. *Thin-Walled Struct.* **2021**, *164*, 107821. [CrossRef]
30. Adeoti, G.O.; Fan, F.; Wang, Y.J.; Zhai, X.M. Stability of 6082-T6 aluminum alloy columns with H-section and rectangular hollow sections. *Thin-Walled Struct.* **2015**, *89*, 1–16. [CrossRef]
31. Wang, Y.Q.; Yuan, H.X.; Chang, T.; Du, X.X.; Yu, M. Compressive buckling strength of extruded aluminum alloy I-section columns with fixed-pinned end conditions. *Thin-Walled Struct.* **2017**, *119*, 396–403. [CrossRef]
32. Yan, J.B.; Kong, G.; Wang, Z.; Zhang, L.; Wang, X. Compression behaviours of aluminum alloy I-column at low temperatures. *Structures* **2022**, *44*, 418–435. [CrossRef]
33. Zhu, J.H.; Li, Z.Q.; Su, M.N.; Young, B. Behavior of aluminum alloy plain and lipped channel columns. *Thin-Walled Struct.* **2019**, *135*, 306–316. [CrossRef]
34. Roy, K.; Chen, B.S.; Fang, Z.Y.; Uzzaman, A.; Chen, X.; Lim, J.B.P. Local and distortional buckling behavior of back-to-back built-up aluminum alloy channel section columns. *Thin-Walled Struct.* **2021**, *163*, 107713. [CrossRef]
35. Chang, Y.C.; Liu, M.; Wang, P.J.; Li, X.L. Behaviors and design method for distortional buckling of thin-walled irregular-shaped aluminum alloy struts under axial compression. *Eng. Struct.* **2017**, *153*, 118–135. [CrossRef]
36. Zuo, W.; Chen, M.T.; Chen, Y.; Zhao, O.; Cheng, B.; Zhao, J. Additive manufacturing oriented parametric topology optimization design and numerical analysis of steel joints in gridshell structures. *Thin-Walled Struct.* **2023**, *188*, 110817. [CrossRef]
37. Tsavdaridis, K.D.; Efthymiou, E.; Adugu, A.; Hughes, J.A.; Grekavicius, L. Application of structural topology optimisation in aluminum cross-sectional design. *Thin-Walled Struct.* **2019**, *139*, 372–388. [CrossRef]
38. Marinopoulou, E.; Tsavdaridis, K.D.; Efthymiou, E. Modern Design Methods on Optimised Novel Aluminum Profiles. *Buildings* **2022**, *12*, 1904. [CrossRef]
39. Georgantzia, E.; Gkantou, M.; Kamaris, G.S. Aluminum alloy channel columns: Testing, numerical modelling and design. *Thin-Walled Struct.* **2023**, *182*, 110242. [CrossRef]
40. Chen, G.; Li, P.; Bao, H.; Huang, Y.; Liu, C.; Zhang, T.; Xiong, G. Design method for axially compressed H-sectional aluminium alloy slender column based on CSM. *Thin-Walled Struct.* **2024**, *205*, 112417. [CrossRef]

41. Schafer, B.W.; Peköz, T. Direct strength prediction of cold-formed steel members using numerical elastic buckling solutions. In *Proceeding of 14th International Specialty Conference on Cold-Formed Steel Structures, St. Louis, MO, USA, 15–16 October 1998*; University of Missouri-Rolla: Rolla, MO, USA, 1998; pp. 69–76.
42. Schafer, B.W. *Distortional Buckling of Cold-Formed Steel Columns*; August Final Report to the American Iron and Steel Institute; American Iron and Steel Institute: Washington, DC, USA, 2000.
43. Schafer, B.W. Local, distortional, and Euler buckling of thin-walled columns. *J. Struct. Eng.* **2002**, *128*, 289–299. [CrossRef]
44. Zhu, J.H.; Young, B. Tests and Design of Aluminium Alloy Compression Members. *J. Struct. Eng. ASCE* **2006**, *132*, 1096–1107. [CrossRef]
45. Gardner, L.; Fieber, A.; Macorini, L. Formulae for Calculating Elastic Local Buckling Stresses of Full Structural Cross-Sections. *Structures* **2019**, *17*, 2–20. [CrossRef]
46. Gardner, L. The continuous strength method. *Proc. ICE—Struct. Build.* **2008**, *161*, 127–133. [CrossRef]
47. Gardner, L.; Wang, F.; Liew, A. Influence of strain hardening on the behavior and design of steel structures. *Int. J. Struct. Stab. Dyn.* **2011**, *11*, 855–875. [CrossRef]
48. Afshan, S.; Gardner, L. The continuous strength method for structural stainless steel design. *Thin-Walled Struct.* **2013**, *68*, 42–49. [CrossRef]
49. Buchanan, C.; Gardner, L.; Liew, A. The continuous strength method for the design of circular hollow sections. *J. Constr. Steel Res.* **2016**, *118*, 207–216. [CrossRef]
50. Liew, A.; Gardner, L. Ultimate capacity of structural steel cross-sections under compression bending and combined loading. *Structures* **2015**, *1*, 2–11. [CrossRef]